Investigating 2D Modeling of Atmospheric Convection in the PBL

C.-H. MOENG

National Center for Atmospheric Research, Boulder, Colorado*

J. C. MCWILLIAMS

National Center for Atmospheric Research, Boulder, Colorado, and Department of Atmospheric Sciences, University of California, Los Angeles, Los Angeles, California*

R. ROTUNNO AND P. P. SULLIVAN

National Center for Atmospheric Research, Boulder, Colorado*

J. WEIL

Cooperative Institute for Research in Environmental Sciences, University of Colorado, Boulder Colorado

(Manuscript received 22 November 2002, in final form 17 October 2003)

ABSTRACT

The performance of a two-dimensional (2D) numerical model in representing three-dimensional (3D) planetary boundary layer (PBL) convection is investigated by comparing the 2D model solution to that of a 3D large-eddy simulation. The free convective PBL has no external forcing that would lead to any realizable 2D motion, and hence the 2D model represents a parameterization (not a simulation) of such a convective system. The present solutions show that the fluxes of conserved scalars, such as the potential temperature, are somewhat constrained and hence are not very sensitive to the model dimensionality. Turbulent kinetic energy (TKE), surface friction velocity, and velocity variances are sensitive to the subgrid-scale eddy viscosity and thermal diffusivity in the 2D model; these statistics result mostly from model-generated hypothetical 2D plumes that can be tuned to behave similarly to their 3D counterparts. These 2D plumes are comparable in scale with the PBL height due to the capping inversion. In the presence of shear, orienting the 2D model perpendicular to the mean shear is essential to generate a reasonable momentum flux profile, and hence mean wind profile and wind-related statistics such as the TKE and velocity variances.

1. Introduction

Two-dimensional (2D) numerical modeling of 3D atmospheric convection can be traced back to the early 1960s (e.g., Lilly 1962; Ogura 1962) when computer power was rather limited. Today, even with advanced supercomputers, certain 3D atmospheric convection problems remain too large for 3D calculation and hence the 2D numerical approach is still widely used for some atmospheric 3D convection. The most notable example is the so-called 2D cloud resolving model (CRM) used to ''simulate'' precipitating cumulus convection in the Tropics (e.g., Tao et al. 1987; Krueger 1988; Xu et al. 1992; Grabowski et al. 1996; Xu and Randall 1996), midlatitude clouds (e.g., Kopp and Orville 1994), and shallow convection in the planetary boundary layer (PBL; e.g., Krueger and Bergeron 1994; Krueger et al. 1995; Wyant et al. 1997; Stevens et al. 1998). These models have been adopted by the Global Energy and Water Cycle Experiment (GEWEX) Cloud System Study (GCSS) community to generate a database for validating and improving single-column cloud parameterizations used in climate models (Randall et al. 2003a). The success of 2D CRMs has led to a recently proposed ''superparameterization'' in climate models (Grabowski and Smolarkiewicz 1999; Khairoutdinov and Randall 2001; Randall et al. 2003b), whereby a 2D CRM is embedded at every horizontal grid point and replaces the traditional single-column cloud parameterization. For many atmospheric applications, the development of 1D convection schemes is considered at a ''deadlock'' (Randall et al. 2003b); 3D cloud resolving models work well but are too computationally expen-

* The National Center for Atmospheric Research is sponsored by the National Science Foundation.

Corresponding author address: Dr. Chin-Hoh Moeng, MMM Division, NCAR, P.O. Box 3000, Boulder, CO 80307-3000.
E-mail: moeng@ucar.edu

sive, and therefore 2D modeling becomes a compromise for representing convection in those applications.

Broadly we may classify 2D models into two categories: The first, which we refer to as 2D ensemble-mean closure modeling, uses an ensemble-mean turbulence model to parameterize *all* of the 3D turbulent motions and is meant to simulate inherent mean 2D features of the convection, which exist in particular applications. This kind of 2D modeling has been extensively used in the meteorological community to simulate flows such as squall lines, convective rolls, or sea-breeze circulations along a straight coast. This type of 2D modeling has a theoretical base; its governing equations can be derived by line averaging (to represent ensemble averaging of) the Navier–Stokes equations along the direction of uniform 2D forcing, so its resolved-scale flow represents the forced 2D motion while the ensemble effect of all 3D turbulence is parameterized. In this study we will focus on PBL convection where no preferred 2D motion exists in any horizontal direction (although the shear convection case studied here has some insignificant 2D features) and hence our investigation does not address this class of 2D modeling; in fact there is no point in using a 2D model of this class for the convection-dominated PBL, because its ensemble mean produces little or no horizontal variation in the flow field; that is the only variation of the ensemble-mean solution is in the vertical.

The second category of 2D models we investigate here will be called 2D turbulence (2DT) models where a subgrid-scale (SGS) model is used to represent the nonresolved motion. The choice of the length and velocity scales in the SGS representation for a 2DT model is still debatable and requires further investigation. A 2DT model intends to capture the characteristics of 3D convection, where the ''resolved'' 2D flow is supposed to carry most of the turbulent energy and fluxes while its SGS model is supposed to represent only a small portion of the ensemble-mean statistics. We would classify many of the previous studies of 2D modeling of PBL turbulence and clouds (e.g., Grabowski and Clark 1991; Wyant et al. 1997; Stevens et al. 1998; and the 2D models shown in Moeng et al. 1996) to be in this category because of their intention to capture (or resolve) the energy-containing turbulent eddies. [In fact, some 2DT models use no explicit SGS model at all; they argue that numerical truncation of monotone algorithms can serve as an effective implicit SGS model (e.g., Grabowski et al. 1996).] The governing equations of a 2DT model cannot be formally derived from the conservation equations of fluid mechanics for 3D turbulent flows, unlike large-eddy simulation (LES; which by definition is a simulation of a 3D turbulent flow), where the equations are firmly based on the Navier–Stokes equations (e.g., Moeng and Sullivan 2002). For a horizontally homogeneous convection system, such as the free convective PBL, no averaging or filtering procedure can be applied to the governing equations to eliminate a y dependence of the flow field and still retain an x dependence. We will discuss the governing equations further in section 2.

In this study, we show that some of the success of 2DT modeling, like the vertical distribution of the total heat flux, may be obvious, but other properties such as obtaining reasonable turbulent kinetic energy (TKE), surface friction velocity, convective mass flux, as well as the characteristic size of 2D plumes, require a deeper examination.

As a first step, we will use the simplest convection system in the atmosphere, namely dry convection in the PBL, as an example. Dry convection in the PBL is analogous to tropical deep convection in some ways: PBL thermals and tropical deep clouds are both forced by surface heating, are capped by a strong inversion, their convective circulations are random in space and time, and in most situations they have no 2D external forcing. However, the PBL convection studied here is cloud free and consists of only turbulent motions dominated by nonlinear dynamical processes, rather than by physical processes like radiation, cloud microphysics, precipitation, and mesoscale variations that occur in tropical deep convection. Therefore, the application of the present study to deep moist convective systems is not direct; however, we believe it shows that further study is needed to investigate how 2D CRMs represent deep moist convection. There are prior studies that examine the performance of 2D CRMs (e.g., Tao et al. 1987; Grabowski et al. 1998; Tompkins 2000), but because of complexity from moist physical processes it is difficult to isolate the mechanisms that led to the similarities and differences between 2D and 3D results. Using the dry convective PBL allows us to look closely into mechanisms responsible for the behavior of a 2DT model. More importantly, there are well-known properties of the PBL turbulence (e.g., wind shear always generates turbulent kinetic energy and the dissipation rate is controlled by the energy-containing scale) that can be used to judge the performance of a 2DT model.

The LES technique will be used as a baseline 3D calculation (and hence is referred to as the 3D model) against which the 2DT model results will be judged. In section 2, we will discuss the origins of the governing equations and physical aspects of the resolved and unresolved scale of motions in LES and 2DT models, and also describe the numerical setup and the convective cases to be studied. The result of the free convective PBL will be given in section 3 and that of a shear convective PBL in section 4. The summary and conclusions will be presented in section 5. In this study, we will focus on convection-dominated turbulent flows only; we will not look at shear-dominated cases because these flows are dominated by coherent vortex dynamics and hence cannot possibly be simulated in any 2D model. We will also not argue whether 2D modeling provides better or worse statistics than 1D modeling; such an argument may depend on the type of 1D model, the type

of convective flows, and also the specific statistical properties in which one is interested. (In this paper we often use the word ''convection'' to mean ''turbulence.'' In meteorological terms, convection is often referred to as moist convection, i.e., cumulus clouds; in this study we use convection loosely to mean buoyantly driven thermals, plumes, updrafts, or their associated circulations.)

2. LES and a 2DT model

a. Governing equations

It is necessary to first review the governing equations and the aspects of SGS physics in LES in order to discuss those of 2DT models. The governing equations of an LES model are derived by applying a spatial filter to the Navier–Stokes equations of an incompressible fluid, which yields

$$\frac{\partial \tilde{u}_i}{\partial t} + \tilde{u}_j\frac{\partial \tilde{u}_i}{\partial x_j} = +\frac{g_i}{T_0}\tilde{\theta} - f\epsilon_{ij3}\tilde{u}_j - \frac{1}{\rho_0}\frac{\partial \tilde{p}}{\partial x_i} - \frac{\partial \tau_{ij}}{\partial x_j} + \nu\frac{\partial^2 \tilde{u}_i}{\partial x_j^2}, \quad (1)$$

where the resolved-scale velocity field $\tilde{u}_i \equiv \iiint_{\text{volume}} (u_i G)dx\,dy\,dz$; G is a spatial filter function; $\tau_{ij} \equiv \widetilde{u_i u_j} - \tilde{u}_i\tilde{u}_j$ is the subfilter-scale (SFS) stress tensor; g_i is the gravitational acceleration, which is nonzero only in the z direction; T_0 is the temperature of some reference state; f is the Coriolis parameter; ϵ_{ij3} is the Levi–Civita tensor; $\tilde{p}$ the resolved-scale pressure fluctuations; and ν the kinematic viscosity of the fluid. The filter width used in G determines the scale of the resolved motion, which is typically chosen to be much smaller than the energy-containing eddy size. The eddies that are retained in (and hence explicitly calculated by) the above filtered governing equations are energy-containing large eddies that are random in space and time. The unresolved small-scale eddies, with velocities $u_i'' \equiv u_i - \tilde{u}_i$, are called SFS motions, and their net effect is represented by the fourth term on the right-hand side. In geophysical turbulent flows, such as atmospheric convection, where the Reynolds number is extremely large, the molecular viscosity term, the last term in Eq. (1) can be neglected because it is several orders of magnitude smaller than the other terms.

As for the governing equations of a 2DT model, there is no theoretical basis to separate the resolved scale and SGS.[1] One may attempt to derive such a set of equations by averaging the Navier–Stokes equations along y to eliminate the y derivatives. However, averaging along one horizontal direction in a horizontally homogeneous field produces a result that is invariant with respect to the other direction. For example, for free convection (no mean wind) in the PBL where the surface forcing is uniform in x and y, a line averaging (in y) would yield a set of equations that contain no variations in either x or y (i.e., an ensemble average set of equations). However, in most 2D modeling applications, the spatial x variations are crucial; these variations are supposed to be representive of resolved-scale convective circulations. Here, we will simply assume that the governing equations for our 2DT model are the same as Eq. (1), except that all of the y derivatives are zero. In this 2D model, the velocity field still has three components: u, v, and w.

b. SFS (or SGS) representation

The physical aspects of the SFS modeling in LES is the following. The solution to Eq. (1) requires a closure model for the stress term, $\partial\tau_{ij}/\partial x_j$. In LES, this term is well defined because of the filtering procedure and represents the effect of small-scale eddies that are eliminated by this procedure. The two most commonly used SFS models in the PBL–LES community are Smagorinsky and Lilly's eddy viscosity model (Lilly 1967) and Deardorff's TKE model (Deardorff 1980), which are similar approaches since both are based on SFS energy budgets. In this study, we adopt Deardorff's TKE model, wherein the SFS stress (τ_{ij}) and heat flux ($\tau_{\theta i}$) are parameterized by an eddy diffusion relationship as

$$\tau_{ij} = -K_M\left(\frac{\partial \tilde{u}_i}{\partial x_j} + \frac{\partial \tilde{u}_j}{\partial x_i}\right), \quad (2)$$

$$\tau_{\theta i} = -K_H\frac{\partial \tilde{\theta}}{\partial x_i}, \quad (3)$$

where the SFS eddy viscosity K_M and diffusivity K_H are determined by the SFS kinetic energy e via

$$K_M = c_K l\sqrt{e}, \quad \text{and} \quad (4)$$

$$K_H = [1 + (2l/\Delta s)]K_M. \quad (5)$$

Here, c_K is a viscosity parameter to be determined and l is equal to the filter width Δs in the absence of stable stratification. Because the filter width varies among the runs, we define an eddy viscosity length scale $l_{\text{vis}} \equiv c_K l$, which is a useful parameter in analyzing the results. The SFS TKE e is solved from the following equation:

$$\frac{\partial e}{\partial t} = -\frac{\partial \tilde{u}_j e}{\partial x_j} - \frac{\partial(\widetilde{u_j'' e} + \widetilde{u_j'' p''})}{\partial x_j} - \tau_{ij}\frac{\partial \tilde{u}_i}{\partial x_j} + \frac{g}{\theta_0}\tau_{\theta 3} - \epsilon, \quad (6)$$

where the molecular dissipation rate is parameterized as

$$\epsilon = c_\epsilon e^{3/2}/l, \quad (7)$$

[1] Since the equations are not derived based on a formal filtering procedure, it is not accurate to call the τ_{ij} term in a 2D model an SFS term. Hereafter, when referring to the 2DT model, we will call the stress tensor an SGS term, rather than an SFS term.

and c_ϵ is a dissipation parameter to be determined. The transport term (second term on the right-hand side) is typically small and parameterized by a simple downgradient diffusion process.

There are two SFS parameters c_K and c_ϵ that must be determined before the above set of equations are closed. If the LES filter cutoff lies within the inertial subrange, these parameters can be derived using inertial subrange theory, which yields $c_K \approx 0.1$ and $c_\epsilon \approx 0.93$ (Moeng and Wyngaard 1989). With these constants, the SFS motion in LES then provides the *statistically* correct energy drainage to dissipation. (We note that in LES implementations, the above SFS model is used locally at every grid point and time step; thus, even though the model may provide the correct net energy drainage, it is likely to misrepresent some of the local effects of the SFS motions.)

The premise of LES is that if the filter scale lies within the inertial subrange, the SFS motion contains only a small amount of energy and performs a small amount of transport; the overall statistics of the LES flow should then be *insensitive* to the SFS closure assumptions. This premise breaks down if the SFS motion contains most of the energy and does most of the transport, which happens when the filter scale is near the energy peak, such as near the wall region in the PBL.

The above premise also breaks down if one uses a 2DT model. With the 2D version of Eq. (1), there is no physical interpretation as to which motions are explicitly calculated and those which are not. Thus, the SGS term in a 2DT model is as equally ill-defined as its governing equations. Here, in our 2D model, we adopt the same SGS concept as the LES and use Deardorff's SGS model to parameterize all unresolved parts of the flow. However, given the ambiguity associated with the unresolved motion, we allow the SGS model parameters to be adjusted in the 2D model. Because there is no way to trace the roots of the governing equations of a 2DT model applied to 3D convection back to any set of fluid dynamic equations, 2DT modeling for such applications should be considered only as a parameterization scheme (i.e., a model, not a simulation) for 3D convection.

c. Numerical setup

The 3D LES runs in this study used $200 \times 200 \times 100$ grid points in a numerical domain of 7.5 km $\times$ 7.5 km $\times$ 2 km. For most of the 2D runs, we used 600×150 grid points to cover a domain of 7.5 km in x and 3 km in z, so the grid size $\Delta z = 20$ m was the same in the 3D and 2D runs, but Δx in 2D runs was 1/3 of that in the 3D runs. We used a sharp wave cutoff filter in x–y with an upper 1/3 wave cutoff to eliminate aliasing errors. Thus, our filter width in the 3D runs is $\Delta s = [(3/2)\Delta x \times (3/2)\Delta y \times \Delta z]^{1/3} \sim 40$ m, and in the 2D runs is $\Delta s = [(3/2)\Delta x \times \Delta z]^{1/2} \sim 20$ m. The difference in resolution between 3D and 2D models will affect our choice of SGS parameter as discussed later. (We chose a finer grid in x for the 2D runs because most 2D modelers would argue that an advantage of using a 2D code is its capability of using a finer grid in x compared to 3D modeling. Furthermore, using 600 grid points gives us a larger data sample to compute statistics. We also performed 2D runs with only 200 grid point in x and found no significant difference from those with 600 grid points.) A larger domain in z is needed for the 2D runs because the PBL sometimes grew beyond the 2-km vertical domain during the simulation period.

Here, we examine two convective PBL regimes. The first is the simplest convective system in the atmosphere, the free convective PBL where the mean wind is zero, and hence, only buoyancy is driving the turbulence. The surface heat flux was fixed at 240 W m^{-2}, and the geostrophic wind was set to 0. The second regime is a convective PBL with shear, where shear also plays a role in generating and maintaining turbulence. There, we used a constant surface heat flux of 100 W m^{-2} and a geostrophic wind of $U_g = 10$ m s^{-1} and $V_g = 0$ m s^{-1}. We also ran a 2D shear convection case with $U_g = 0$ m s^{-1} and $V_g = 10$ m s^{-1}, such that the 2D domain was perpendicular to the geostrophic wind. These shear convection cases are designed to show the sensitivity of the 2DT solution to the orientation of the 2DT model domain.

3. Free convective PBL

a. LES

We first ran a baseline calculation of a free convective PBL using the National Center for Atmospheric Research (NCAR) LES code, which is denoted as F-3D. This case has been well simulated by the LES community and its statistics are well documented (e.g., Schmidt and Schumann 1989; Nieuwstadt et al. 1993). The flow features and statistics generated by LES have been shown to compare well with field measurements and convection tank experiments (Willis and Deardorff 1979). A distinct flow feature of free convection is an irregular 3D cellular pattern that forms near the heated surface, where narrow peripheries of the cells are convergence lines of the horizontal flow (e.g., Willis and Deardorff 1979; Schmidt and Schumann 1989). Intersections of these convergence lines are typical locations of vigorous convective updrafts, which often extend throughout the whole PBL. The flow field is statistically homogeneous in the horizontal directions without any preferred 2D motion.

Figure 1 shows a vertical cross section of the 3D LES flow field, in an x–z domain at an instant in time (here we chose the flow field at hour 4). At this time, the PBL depth is about 1.2 km. The flow field is random in space and time and there is no correlation between the horizontal velocity fluctuations u and the vertical velocity w; this lack of correlation is expected for free convection where the net momentum fluxes are 0. A few strong

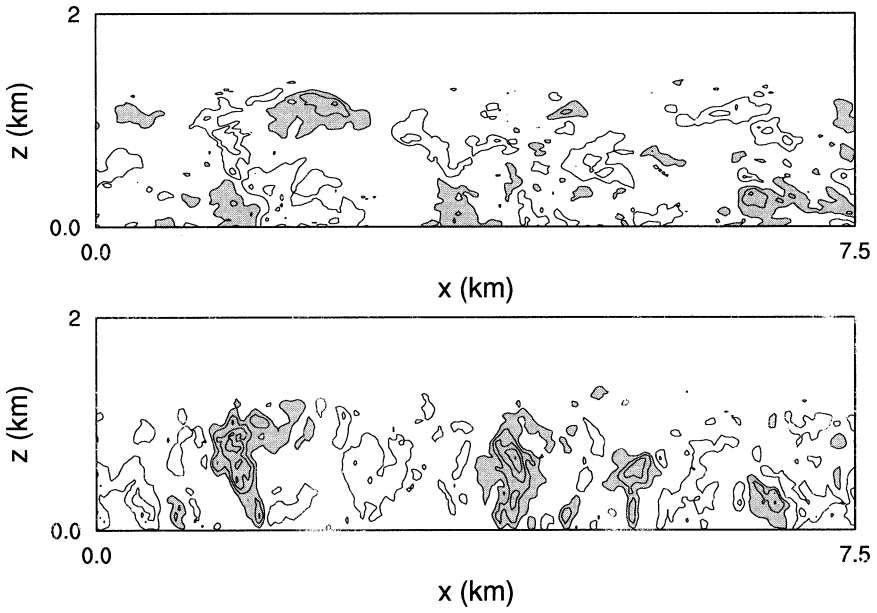

FIG. 1. Contours of (top) u and (bottom) w fluctuations in an x–z cross section at hour 4 of F-3D simulation. The contours are -5, -4, -3, -2, -1, 1, 2, 3, 4, 5 m s^{-1}; and the gray area represents positive contours.

updrafts extend all the way to the PBL top and have a characteristic size on the order of the PBL depth.

The time evolution of the PBL depth, the layer-averaged (over the whole PBL) TKE, and the surface friction velocity u_* from the 3D run are shown as thick solid lines in Fig. 2. The so-called minimum friction velocity u_* is due to convective circulations in this free shear case and is about $0.1w_*$, which agrees with previous studies (e.g., Schmidt and Schumann 1989). In this case, the convective velocity scale $w_* \equiv [(g/T_0)\overline{w\theta}_0 z_i]^{1/3}$ is about 2 m s^{-1}, where $\overline{w\theta}_0$ is the surface heat flux, an overbar represents an ensemble average, and z_i is the PBL depth. Even though the layer-averaged TKE increases slightly with time, the simulated turbulence can be considered quasi steady after about 30 min of simulation.

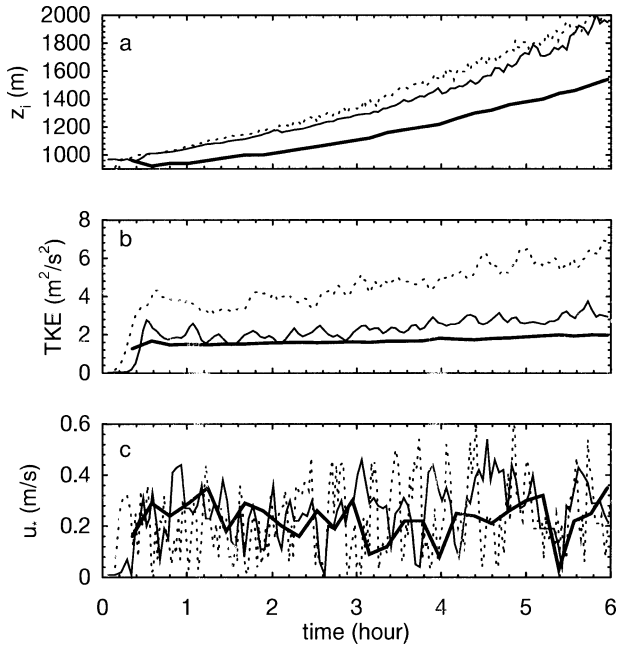

FIG. 2. Time evolution of (a) PBL height, (b) layer-averaged TKE, and (c) surface friction velocity for the free convective case. Thick solid lines are from F-3D, dotted lines from F-2D-A, and thin solid lines from F-2D-B.

The vertical profiles of the heat flux, TKE, and velocity variances (see Fig. 3) serve as standard statistics to evaluate the performance of 2D runs. These ensemble-mean statistics profiles were obtained by first averaging correlations over an x–y plane, mapping the instantaneous profiles onto the normalized height coordinate z/z_i, and then averaging them over a time period between hours 2 and 6. Notice that most of the heat flux and TKE come from the resolved scale motion. Bulk properties, such as the minimum heat flux at the PBL top (which is about -0.16 of the surface heat flux), the uniformity of the TKE in height (0.40–$0.5w_*^2 \sim 1.6$–2.0 m^2 s^{-2}), the equivalence of the two horizontal-velocity variances ($\sim 0.2w_*^2 \sim 0.8$ m^2 s^{-2}) and the height and the magnitude of the w-variance maximum ($\sim 0.5w_*^2 \sim 2$ m^2 s^{-2}), all agree well with field measurements (Lenschow et al. 1980), laboratory tank data (Willis and Deardorff 1974), and previous LESs (Nieuwstadt et al. 1993).

b. 2D run with $c_K = 0.1$

The first 2D run, denoted as F-2D-A, used the TKE SGS model with the same parameters $c_\epsilon = 0.93$ and

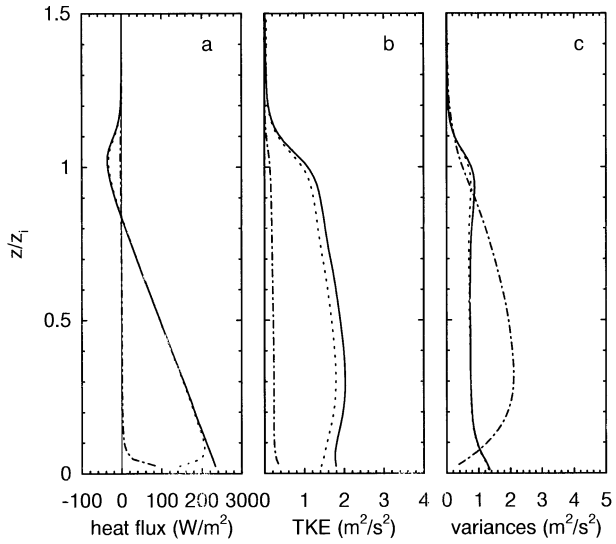

FIG. 3. Vertical profiles of (a) the heat fluxes (total as solid line; resolved scale as dotted line; SFS as dotted–dashed line), (b) TKE (total as solid line; resolved scale as dotted line; SFS as dotted–dashed line), and (c) resolved-scale velocity variances ($\overline{u^2}$ as solid line; $\overline{v^2}$ as dotted line; $\overline{w^2}$ as dotted–dashed line) from F-3D.

$c_K = 0.1$ as the LES. The flow field at hour 4 of this 2D run is shown in Fig. 4. It is clear that the 2D convective updrafts are much stronger than the 3D result, shown in Fig. 1.

This strong convection is reflected in the time evolution of the PBL depth, the layer-averaged TKE, and u_*, shown as dotted curves in Fig. 2. The F-2D-A case grows too rapidly and produces too much layer-averaged TKE compared to the LES. The entrainment rate (computed from the slope of the final 4 h of the simulation period) is about 6.7 cm s^{-1} in F-2D-A versus ~4.6 cm s^{-1} in the LES. The average friction velocity is reasonable but it fluctuates more in the 2D case (partially due to sampling errors because the averaging was performed over only 600 grid points in x instead of over x–y plane like in the LES); on average it is also about $0.1w_*$.

A quick glance at the heat flux profile from F-2D-A (Fig. 5a) shows similar features to that of the 3D run (Fig. 3a). Although the entrainment heat flux from F-2D-A is twice as large as that from the 3D run, the overall shape of the heat flux profile agrees with the 3D result. This similarity is easy to explain. When turbulence reaches its quasi-steady state, the flux profile of any conserved variable, such as potential temperature, is always linear with height because $\partial/\partial t(\partial\Theta/\partial z) = -\partial^2\overline{w\theta}/\partial z^2 = 0$. Thus, for a given surface heat flux, the profile depends only on its entrainment flux, which, for the free convective PBL, is around -0.2 of the surface flux (e.g., Tennekes 1973). The entrainment heat flux value is constrained somewhat by the fact that only a small percentage of the buoyancy source is used to entrain warm air from above while most of it is destroyed by dissipation (Ball 1960). This so-called energy efficiency of the entrainment process is probably not too different regardless of 2D or 3D modeling. Thus, the heat flux profile is a rather robust statistical property, and this may extend to vertical fluxes of other conserved scalars, such as moisture.

Figure 5b shows the vertical distribution of TKE, which is grossly overestimated throughout the bulk of the PBL by comparison to the 3D results. (Note that Figs. 5b–5c use scales 2 times larger than Figs. 3b–3c.) Almost all of the TKE resides in the resolved scale where the thermally induced 2D updrafts are too vig-

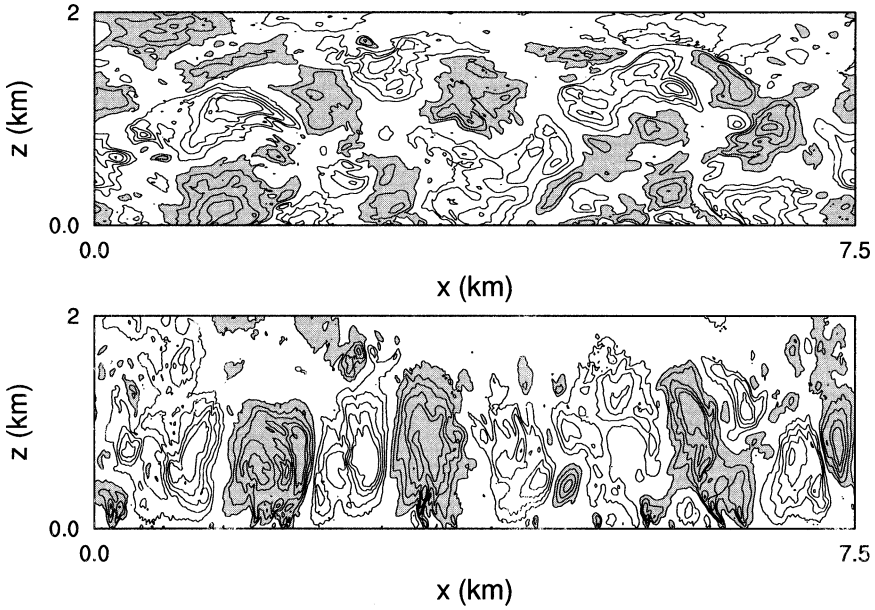

FIG. 4. Same as Fig. 1, except for F-2D-A.

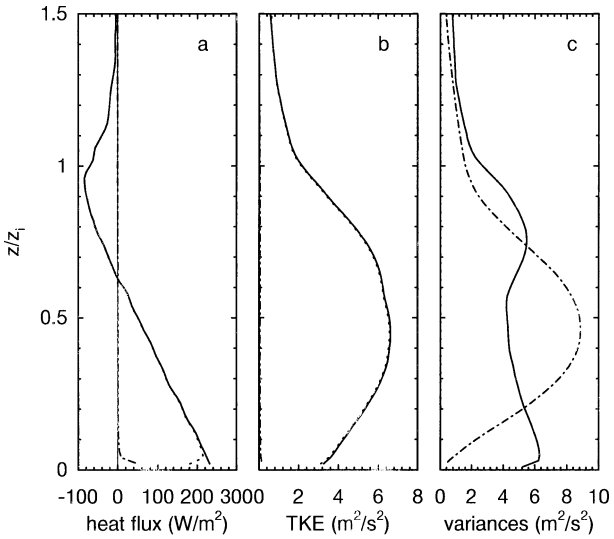

FIG. 5. Same as Fig. 3, but from F-2D-A.

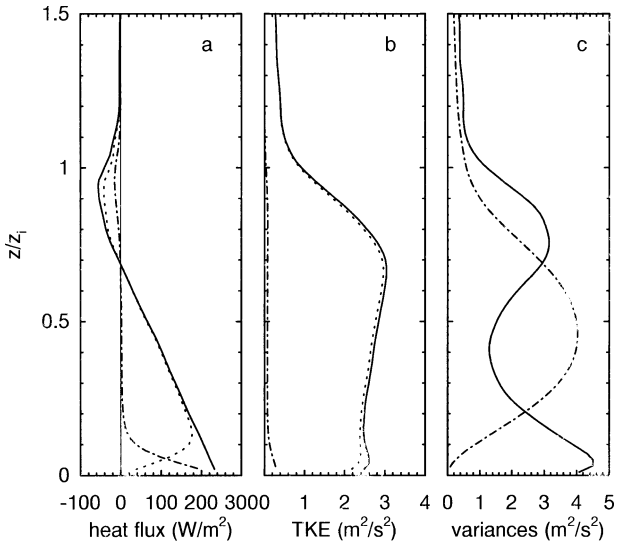

FIG. 6. Same as Fig. 3, but from F-2D-B.

orous, as revealed in Fig. 4. Figure 5c shows that the v variance is negligibly small, while u and w variances are much too large compared to those in the LES. There is a tendency for a 2DT model to produce a w variance peaking at mid-PBL and decreasing symmetrically about this level; the w variance should peak closer to the heat source in the convective PBL, based on field observations (e.g., Lenschow et al. 1980).

Since there is no theoretical model for the SGS motion in this 2DT model, we may empirically adjust its SGS parameters to see if any of the statistical results might be improved. We first varied the dissipation parameter c_ϵ and found that the total TKE was insensitive to this parameter. A decrease in c_ϵ results in a larger SGS TKE e according to Eqs. (6) and (7); however, SGS contributes only a small portion of the total TKE and thus the latter remains about the same.

Tuning the diffusivity parameter c_K, which appears in (4), changes the SGS eddy viscosity K_M (and hence eddy diffusivity K_H), which modifies the resolved-scale flow directly according to (1) and in effect changes the total TKE amount of the 2D model drastically as shown later. Let us first compare the resulting K_M value (which is not a prespecified quantity in our 2D and 3D models, but rather depends on the resulting SGS TKE) in the LES and F-2D-A. In the LES, we used a filter length scale of $l \sim 40$ m and $c_K = 0.1$, and thus the eddy viscosity length scale $l_{\text{vis}} = c_K l \sim 4$ m in the LES run. The SGS energy in the LES solution is about $e \sim 0.15$ m^2 s^{-2} in the bulk interior of the PBL, and this leads to $K_M = l_{\text{vis}}\sqrt{e} \sim 1.5$ m^2 s^{-1}. In F-2D-A, we used a grid length scale of $l \sim 20$ m and $c_K = 0.1$, hence $l_{\text{vis}} \sim 2$ m. The SGS TKE from the F-2D-A run is only about $e \sim 0.04$ m^2 s^{-2}, and this leads to $K_M \sim 0.4$ m^2 s^{-1}, which is about one-fourth of the LES K_M. This smaller eddy viscosity partially explains the larger TKE of the F-2D-A flow, compared to that of the LES.

c. 2D run with $c_K = 1$

By trial and error, we found that increasing c_K tenfold in the 2D model leads to a TKE similar to the LES. In this second 2D run (denoted as F-2D-B), we used $c_K = 1$ (and hence $l_{\text{vis}} \sim 20$ m) and that led to a K_M of about 4 m^2 s^{-1}.

The time evolution for this run is plotted as the thin solid curve in Fig. 2. The entrainment rate for this run is still larger than that of the LES (Fig. 2a), though slightly improved by comparison to the first 2D run. Consistent with our tuning, the layer-averaged TKE is much closer to the LES value. The surface friction velocity is similar to the first 2D run but fluctuates less and compares better with the LES run.

For run F-2D-B, the vertical distributions of heat flux and TKE (Figs. 6a–6b) both agree better with those of the LES (note the horizontal scale is now changed back to be the same as that in Fig. 3), although the TKE is still about 20% larger than that of the LES, but this can be tuned down further. Noted that most of the heat flux and TKE are carried by the resolved-scale motion, that is, the hypothetical 2D plumes, rather than by its SGS model. The individual TKE components (i.e., the velocity variances $\overline{u^2}$, $\overline{v^2}$, and $\overline{w^2}$ shown in Fig. 6c) for this run, however, are still quite different from the LES. In the 2D flow, the v variance is negligibly small, while the streamwise velocity (or u) variance is much too large. The streamwise velocity variance shows local maxima near the surface and the PBL top, which is another clear signature of 2DT model result, suggesting a convective circulation that is more organized than its 3D counterpart. Again, the w variance peaks at the mid-PBL with a symmetrical distribution about the mid-plane. The peak value is about twice that of the LES. Since the convective mass flux (defined as the ratio of the vertical flux of a scalar field to the difference be-

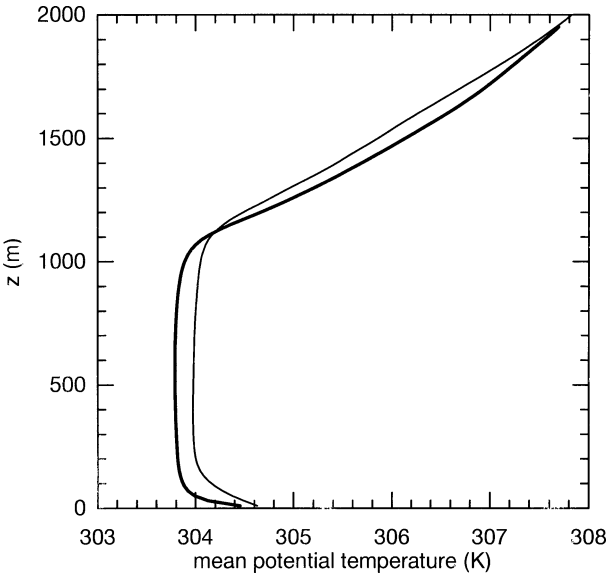

FIG. 7. Vertical profiles of the mean potential temperature computed from F-3D (thick solid line) and F-2D-B (thin solid line) averaged over the last 4 h of simulation.

tween its averaged concentrations within updrafts and downdrafts) is closely tied to the *w* variance (Businger and Oncley 1990; Wyngaard and Moeng 1992), one may want to increase the c_K value even further in a 2DT model to reduce the *w* variance and so get a better representation of convective mass flux.

Figure 7 shows that both F-3D and F-2D-B produce a well-mixed potential temperature profile, which is a unique property of the convective PBL. Because the heat flux remains positive throughout most of the PBL (Figs. 3 and 6), both LES and F-2D-B capture the countergradient heat transfer property of the convective PBL.

d. Characteristic eddy size

Figure 8 shows the instantaneous flow field of F-2D-B using the same contour intervals as those in Fig. 1. The flow field is smoother than that shown in Fig. 1, with a clear absence of small-scale random fluctuations. These hypothetical 2D motions show a characteristic eddy size on the order of the PBL depth, just like their 3D counterparts; this is unexpected and will be discussed next.

Most 2D turbulent flows are known to have an upscale transfer of energy, and hence we might have expected to see much larger energy-containing eddies in the 2DT model than in LES. But Figs. 1 and 8 suggest that the resolved eddy sizes in the 2D and 3D runs are on the order of their own z_i. Since the F-2D-B run has too small a domain to confirm this finding, we ran another case, F-2D-C, where the horizontal domain and the number of grid points in *x* were both increased by a factor of 10; that is, L_x was 75 km and the number of grid points in *x* was 6000, keeping all other parameters the same as the F-2D-B run. The PBL growth rate, TKE, and u_*, as well as the vertical profiles of heat, TKE, and variances all remain about the same as for run F-2D-B, and hence are not shown here.

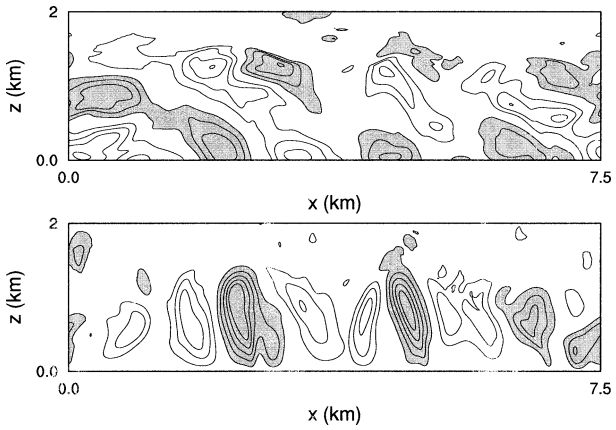

FIG. 8. Same as Fig. 1, except for F-2D-B.

Figure 9 shows contour plots of the flow field from this large domain 2D run; for a direct comparison to the F-2D-B flow, we just show one-tenth of the F-2D-C domain, ranging from 0 to 7.5 km. The dominant eddy size remains on the order of z_i, the depth of the capping inversion.

To show that the resulting 2D flow field does not represent the line-averaged flow of the free convection, we performed a line averaging along *y* on the LES flow field shown in Fig. 1. The magnitude of the fluctuating flow field after such averaging is everywhere less 1 m s^{-1} and hence cannot be shown with the same contour intervals used in Figs. 1 and 8. In fact, the residual small fluctuating field is due to sampling errors because of the limited LES *y* domain, which is only 7.5 km. If the *y* domain in the LES was much larger, the *y*-averaged LES flow field should show no turbulent fluctuations at all in the *x* direction. Thus, the 2D plumes shown in Fig.

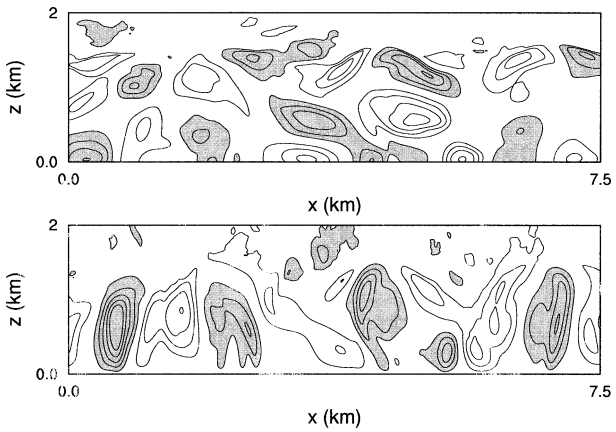

FIG. 9. Same as Fig. 8, except for one-tenth (from 0 to 7.5 km) of the F-2D-C domain.

8 are not representative of the *y*-averaged flow field of 3D convection, but rather they look more like a flow field of an arbitrary *x*–*z* cross section of the 3D convection it tries to represent.

e. The dependence of TKE on SGS viscosity

As shown above, the total TKE and many other statistical properties that are strongly tied to the TKE or the vertical velocity variance generated by the 2DT model depend strongly on the SGS eddy viscosity K_M, which is consistent with earlier studies of 2D modeling of buoyant convection as discussed by Lilly (1967). This strong dependency should not be the case for LES that has SFS eddies lying within the inertial subrange of the spectrum. In the free convective PBL, the total TKE should depend only on the energy input (i.e., the surface heat flux) as explained below. In the ensemble-mean TKE budget equation, the total (volume average over the whole PBL) buoyancy production $\int B\,dz$ is balanced by the total dissipation, and is proportional to the surface heat flux as

$$\int \epsilon\, dz = \int B\, dz \sim 0.4\overline{w\theta}_0 z_i, \tag{8}$$

where the integral is taken over the whole PBL and hence there is no contribution from the pressure and turbulent transport terms. The ϵ and B are the horizontally averaged (i.e., ensemble mean) dissipation and buoyancy terms in the TKE budget. (In deriving the above balance, we assumed that the entrainment buoyancy flux is -0.2 of its surface flux.) Furthermore, due to the energy cascade, the net dissipation rate in 3D turbulence is controlled by the energy-containing eddies, which have a velocity scale $\sqrt{E}$ (E denotes the total TKE) and a length scale z_i, and hence ϵ can be expressed as

$$\epsilon \propto \frac{E^{3/2}}{z_i}. \tag{9}$$

Equations (8) and (9) link the total TKE of the convective system to the surface heat flux or forcing, $\overline{w\theta}_0$. Thus, the total TKE in LES should be independent of the SFS closure assumptions. We ran two more LESs with their c_K either 5 times larger or 5 times smaller than the control run; the overall statistics remain similar and hence are not shown in this paper. (However, the c_K value for LES should not be made to deviate too much from its inertial-subrange-predicted value 0.1.)

On the other hand, Eq. (9) is not valid for 2D flow. What actually controls the total amount of TKE in the 2D modeled convection is the imposed SGS eddy viscosity, which is needed to dissipate energy. A larger SGS eddy viscosity generates less vigorous convective 2D plumes in the 2D model as seen from Figs. 4 and 8.

We also plotted the TKE budgets from F-3D, F-2D-A, and F-2D-B in Fig. 10. The differences in the vertical

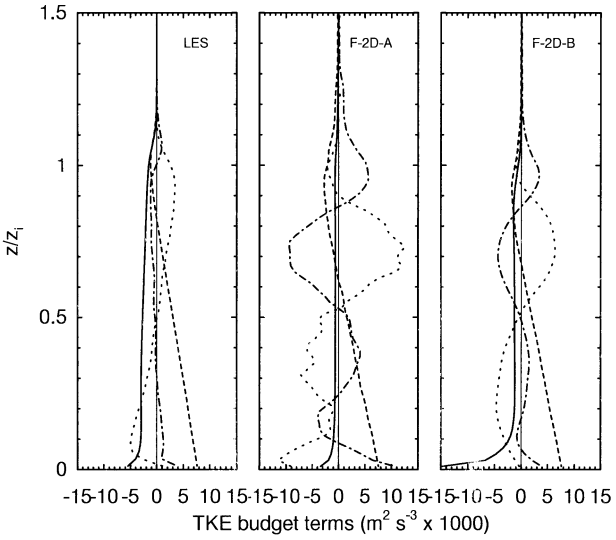

FIG. 10. TKE budgets from LES (F-3D), F-2D-A, and F-2D-B. Dashed curves represent buoyancy production, solid curves represent dissipation, dotted curves for turbulent transport, and dashed–dotted curves for pressure transport.

distributions of these budgets are significant between F-3D and F-2D-A, but less so between F-3D and F-2D-B. The magnitudes of the turbulent and pressure transport terms were greatly overestimated in F-2D-A due to its strong vertical velocity fluctuations.[2]

Evidence showing that (9) does not apply to these 2D flows can be seen by comparing the dissipation terms between F-2D-A and F-2D-B in Fig. 10. The dissipation rate is smaller in F-2D-A than in F-2D-B but the total TKE is much larger in the former (Fig. 2b). This again indicates the lack of energy cascade from energy-containing eddies to SGS and so the SGS dissipation rate of the 2D convection is not controlled by the total TKE.

The lack of the energy cascade process can also be seen from the 1D (along *x*) velocity spectra. Figure 11 compares the *u* and *w* spectra at the mid-PBL between F-3D (thick solid curve), F-2D-A (dotted curve), and F-2D-B (thin solid curve). Most velocity variances in the 2D flows remain at the energy-containing scale (at wavenumber $n = 3$–4, which corresponds to about 2 km in wavelength) compared to the LES flow. Increasing the SGS eddy viscosity from F-2D-A to F-2D-B

[2] In F-2D-A, the buoyancy production is larger than the dissipation rate; the total amount of buoyancy production (i.e., layer integrated) is about 30% larger than the layer-integrated dissipation rate, which is contradictory to (8). This imbalance was compensated by a large numerical dissipation near the surface. Consider and extreme 2D run where c_K was set to 0. There would be no SGS eddy viscosity and the dissipation term (due to SGS model) would be 0. The modeled flow field would either blow up or might survive if there were enough numerical dissipation. We checked the sum of the buoyancy, dissipation, turbulent, and pressure transport terms in F-2D-A; the imbalance resided mainly near the surface presumably because the SGS eddy viscosity there was not large enough to diffuse the flow near the wall and a large numerical effect took place there.

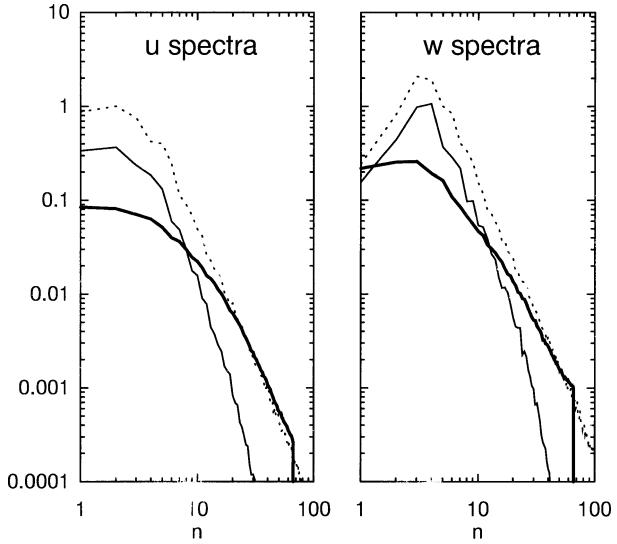

FIG. 11. Velocity spectra in x as functions of normalized wavenumber $n = k_x(L_x/2\pi)$ from F-3D (thick solid curves), F-2D-A (dotted curves), and F-2D-B (thin solid curves).

reduces not only the energy spectra at the high wavenumbers but also that of energy-containing scales. This feature shows up in the flow field; by comparing Figs. 4 and 8 we see that the intensity of the dominant updrafts (energy-containing eddies) is reduced and at the same time the flow field becomes smoother without much small-scale random fluctuations. In LES, changes made to the SFS model should affect only the inertial subrange scales, which carry only a small portion of TKE. The sensitivity of TKE to SGS eddy viscosity is a fundamental difference between LES and 2DT modeling; it is not an artifact of the particular SGS model we use here. [This conclusion may apply only to the modeling of turbulence. According to Xu et al. (1992), the primary kinetic energy sink of tropical deep convection is drag of precipitation, not energy cascade and dissipation.]

With a further increase of c_K in the 2DT model, the 2D convective plumes would become smoother and carry smaller TKE and velocity variances. To estimate roughly the reduction rate of TKE with c_K, we ran a 2D case with $c_K = 5$, which is 5 times larger than that used in F-2D-B; the TKE and the peak value of w variance (not shown) are about half of those from F-2D-B. This dependence of TKE and w variance on the SGS eddy viscosity is consistent with the 2D modeling result reported by Stevens et al. (1998) where they found that the w variance decreases as the grid size increases. An increase of grid size, while keeping c_K the same, also increases the SGS K_M according to (4).

f. The SGS eddy viscosity (and diffusivity) in 2DT modeling

What is the proper amount of SGS eddy viscosity for a 2DT model? Our study shows that the SFS K_M value in the LES is about 1.5 $m^2\ s^{-1}$, and in order to reproduce a similar TKE, our 2DT model requires a SGS K_M of about 4 $m^2\ s^{-1}$. We had expected the SGS K_M in the 2DT model to lie in the midpoint between the LES value (which is 1.5 $m^2\ s^{-1}$ for the resolution we use) and the ensemble-mean value, which is $\sim 0.1 w_* z_i \sim 250\ m^2\ s^{-1}$ in the midlayer of the convective PBL (Wyngaard 1992). However, this study shows that SGS K_M for a 2DT model needs to be much smaller than that of a 1D ensemble-mean model, and its magnitude is comparable to that of LESs. Only then, the hypothetical 2D motion would carry most of the energy and fluxes, as the resolved-scale 3D motion in LES does.

One may wonder whether the c_K value requires further tuning if the surface heat flux is changed. The answer is no. For the free convective PBL regime, we have a standard TKE value to compare to: the TKE normalized by w_*^2 is about 0.4–0.5 in the bulk PBL (except near the wall and the top) regardless of the surface heat flux value. This normalized TKE is observed in field measurements (e.g., Lenschow et al. 1980), laboratory tank data (Willis and Deardorff 1974), and numerous LESs (Nieuwstadt et al. 1993). We performed several more 2D runs of the free convection PBL with varying surface heat flux. We keep $c_K = 1$ and use the same grid resolution as in F-2D-B so the SGS K_M is on the order of 4 $m^2\ s^{-1}$. The normalized TKE values (not shown) of these runs remain at about 0.4–0.5w_*^2, where w_* changes from case to case. In fact, as shown in the next section, even for a convective PBL with mean wind, this eddy viscosity level is still appropriate for the 2DT model.

4. Shear convective PBL

Wind shear complicates the convective system in the PBL; mean shear provides an additional source for turbulence and momentum transfer becomes an issue. Our main purpose here in examining a shear convective PBL is to show how momentum transport is represented in a 2DT model.

a. LES

We first ran a calculation with the LES, case S-3D, which has a surface heat flux of 100 W m^{-2}. (Note that the c_K value used in the LESs is always 0.1.) The stability parameter $-z_i/L$ is about 10, where L is the Monin–Obukhov length; this $-z_i/L$ value represents a moderate to strong convective PBL where buoyancy is still the main turbulence producer, but shear also plays a role, particularly near the surface. The convective velocity w_* for this case is about 1.5 m s^{-1}, and the flow field is still predominantly 3D in nature. We do not discuss the details of the flow here, but merely use the LES results as a baseline case for comparison with the 2D runs.

The time evolution of z_i, layer-averaged TKE, and u_* for the LES result is shown by the thick solid lines in

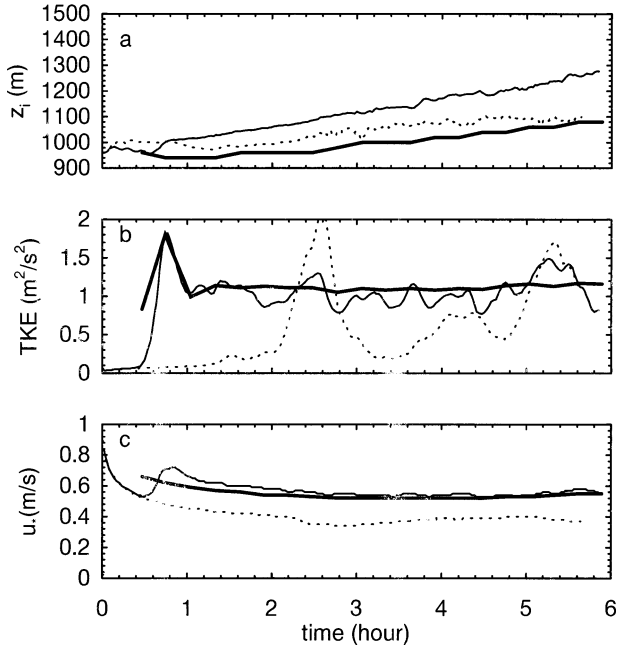

FIG. 12. Time evolution of (a) PBL height, (b) layer-averaged TKE, and (c) surface friction velocity for the shear convective case. Thick solid lines are from S-3D, dotted lines from S-2D-U, and thin solid lines from S-2D-V.

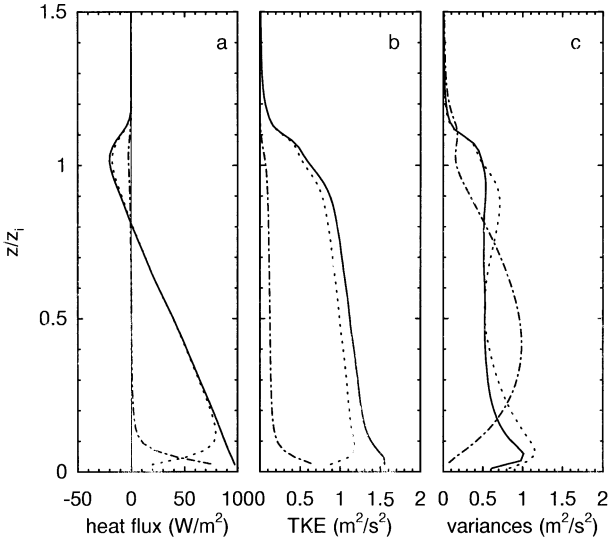

FIG. 13. Vertical profiles of (a) the heat fluxes (total as solid line; resolved scale as dotted line; SFS as dotted–dashed line), (b) TKE (total as solid line; resolved scale as dotted line; SFS as dotted–dashed line), and (c) resolved-scale velocity variances ($\overline{u^2}$ as solid line; $\overline{v^2}$ as dotted line; $\overline{w^2}$ as dotted–dashed line) from S-3D.

Fig. 12, and the vertical profiles of heat flux, TKE, and the velocity variances are given in Fig. 13. The statistics in these figures are similar to those found in previous LESs of shear convective PBLs and field measurements (e.g., Moeng and Sullivan 1994) and for $-z_i/L \sim 10$, they are not significantly different from those of the free convective PBL shown in Fig. 3. The streamwise momentum flux (in this case $\overline{uw}$) and both components of the mean horizontal velocity (U and V) are shown in Fig. 14. The mean wind speed and the mean potential temperature (not shown) are both well mixed over the bulk (upper 90%) of the PBL. The PBL wind veers slightly to the left of the geostrophic wind (in the Northern Hemisphere) due to the Coriolis effect. The streamwise momentum flux is negative throughout the entire PBL because, on average, updrafts tend to carry smaller momentum from the surface, while downdrafts carry larger momentum from above, which is typical of 3D turbulence with shear. The streamwise momentum flux is linear with height, which may be a feature of a quasi-steady state and is similar to conserved scalar fluxes.

b. 2D run with domain parallel to the mean wind

We ran the first 2D case with the domain (x–z) oriented along the geostrophic wind direction with $U_g = 10\ \mathrm{m\ s^{-1}}$ and $V_g = 0\ \mathrm{m\ s^{-1}}$. (In this paper, the streamwise direction is referred to as the geostrophic wind direction, although the mean wind inside the PBL changes direction due to the Coriolis force.) In this case, denoted as S-2D-U, we used $c_K = 1$ so its $l_{\mathrm{vis}} \sim 20$ m, which is the same as it is in the case F-2D-B (for free convection). The PBL growth for S-2D-U (the dotted line in Fig. 12a) compares well with the LES, but that may be artificial as shown later. The layer-averaged TKE (Fig. 12b) fluctuates significantly and on average is smaller than that of the LES. The friction velocity for run S-2D-U (Fig. 12c) is about 30% less than the LES. Unlike the no-shear case, the friction velocity depends mainly on the mean shear near the surface and is less dependent

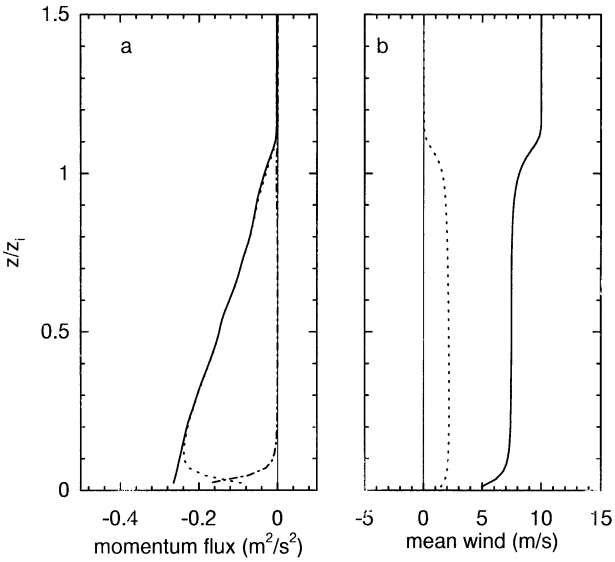

FIG. 14. Vertical profiles of (a) the streamwise momentum fluxes (total as solid line; resolved scale as dotted line; SFS as dotted–dashed line) and (b) the mean wind in streamwise direction (solid curve) and spanwise direction (dotted curve) from S-3D.

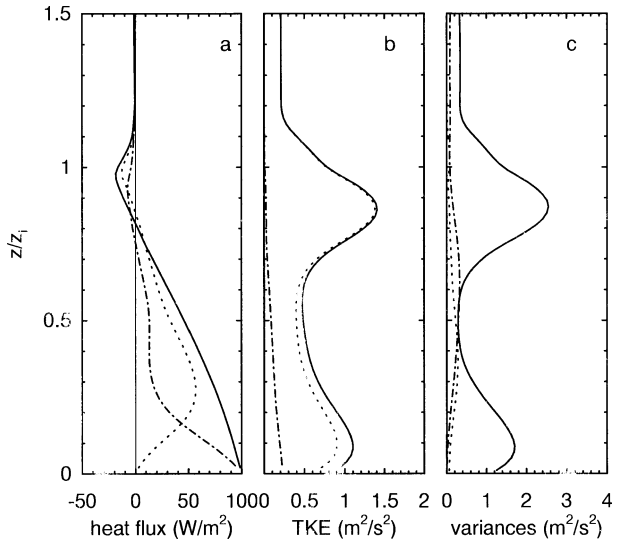

FIG. 15. Same as Fig. 13, but from S-2D-U.

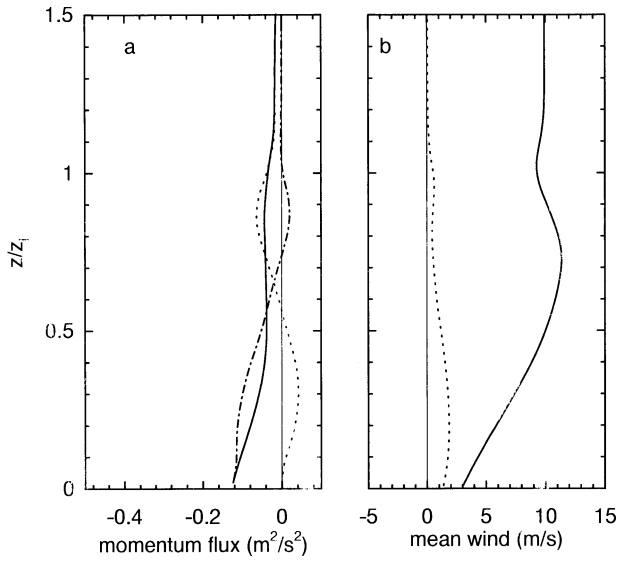

FIG. 16. Same as Fig. 14, but from S-2D-U.

of the convective circulation. The underestimated u_* of S-2D-U is due to a poor momentum flux, which will be shown next.

We now look at the vertical distributions of turbulence statistics from run S-2D-U. The vertical profile of the total heat flux (solid line in Fig. 15a) compares reasonably well with its 3D counterpart (Fig. 13a), as anticipated, although the SGS flux has a major contribution in S-2D-U (see dotted–dashed line). In contrast, the TKE profile (Fig. 15b) is a poor representation of the LES profile (Fig. 13b) and attains a maximum in the upper PBL instead of near the surface; this will be explained later. Furthermore, the individual velocity variances are wrong (comparing Figs. 13c and 15c), with the streamwise velocity component dominating and reaching local peaks near the bottom and the top of the PBL. The v and w variances are greatly underestimated by comparison to the LES results (Fig. 13c).

The streamwise momentum flux from run S-2D-U (Fig. 16a) totally misrepresents the flux from the LES. The most noticeable difference occurs in the resolved-scale flux, which is positive in the 2D flow (dotted line in Fig. 16a) rather than negative as in the LES (compared to dotted line in Fig. 14a). This positive flux has been found before in 2D modeling of convective storms when the 2D domain is aligned with the mean wind (e.g., Lilly 1986) where it was argued that the resolved-scale convective updrafts are tilted downshear vertically and the tilting dominates the resolved motion, such that the resolved-scale u and w become positively correlated. In contrast, the 3D model (LES) is known to generate a momentum flux of opposite sign to its mean shear, such that the latter can produce turbulence energy through the term $-\overline{uw}\partial U/\partial z$ in the TKE budget. [The SGS momentum flux remains downgradient, however, by the eddy viscosity assumption in Eq. (2).]

As a result of the momentum flux problem, the surface friction velocity u_* is underestimated as shown in Fig. 12c, and the mean wind field from the 2D model (Fig. 16b) does not match that in the LES. Instead of a well-mixed profile as in LES, the mean wind increases with height to form a jet in the upper part of the PBL. The jet results in a local maximum of the u variance and TKE at $\sim 0.9z_i$ (Fig. 15); this has no counterpart in the LES.

c. 2D run with domain perpendicular to the mean wind

Changing the orientation of the 2D domain relative to the geostrophic wind drastically improves the 2D results. We ran the second 2D run (denoted as S-2D-V) with a geostrophic wind pointing to the north, $U_g = 0$ m s^{-1} and $V_g = 10$ m s^{-1}, and hence the 2D domain (x–z) is now perpendicular to the geostrophic wind. In this case, the streamwise mean wind is V, and again we keep $c_K = 1$. Convective plumes are allowed to vary only in the x–z plane and hence cannot be tilted by the major vertical shear in y. As a result, the streamwise momentum flux (shown in Fig. 17a) is much improved, being negative throughout the PBL and with a magnitude that decreases linearly with height like its 3D counterpart (Fig. 14a). Without the direct effect from the shear, the upward-moving eddies in S-2D-V tend to carry smaller momentum from below, while downward eddies tend to carry larger momentum from above, just like in the LES flow. Consequently, the mean streamwise velocity profile is simulated well (cf. solid lines in Figs. 14b and 17b) and is well-mixed in the bulk of the PBL. The spanwise mean wind (shown as dotted line), though having a different sign from that shown in Fig. 14b, is actually well captured because, in this case, the streamwise velocity is V and the PBL wind

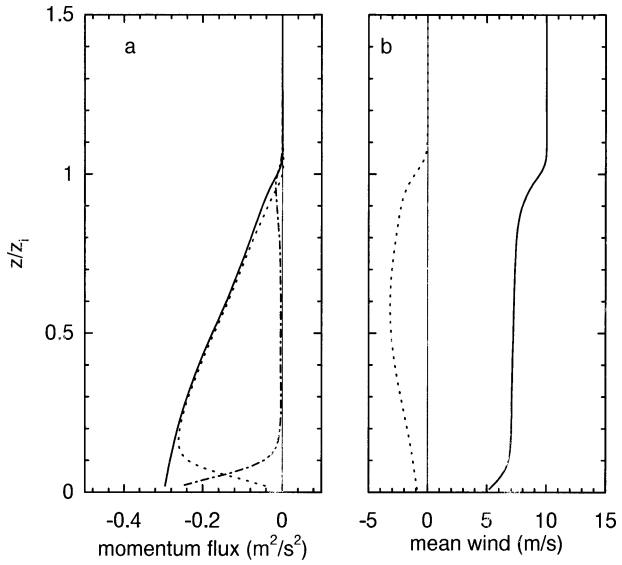

FIG. 17. Same as Fig. 14, but from S-2D-V.

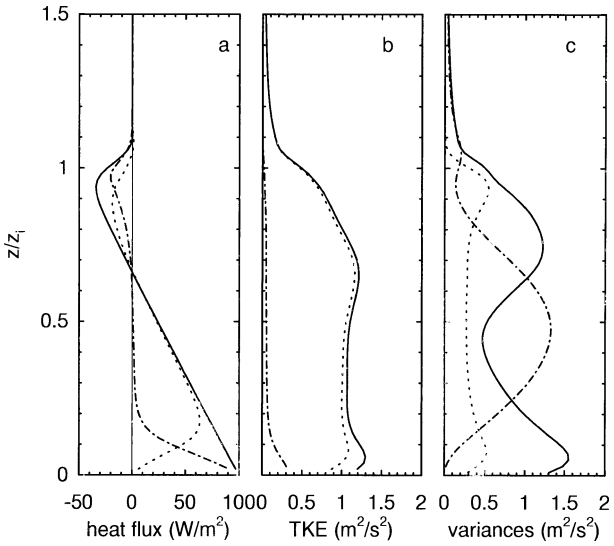

FIG. 18. Same as Fig. 13, but from S-2D-V.

veers slightly to the left of the geostrophic wind V_g, just like Fig. 14b where the PBL wind veers slightly to the left of U_g. One of the most important differences from S-2D-U is that with the streamwise momentum flux and the streamwise mean shear having opposite signs (mainly near the surface), the shear in S-2D-V serves as a production for turbulence, as it should for the PBL flow.

The improvement in the momentum transport also leads to better representations of other wind-related statistics in the 2D model; this includes the layer-averaged TKE (thin solid curve in Fig. 12b), the surface friction velocity (thin solid curve in Fig. 12c) and the vertical distributions of heat flux, TKE, and velocity variances shown in Fig. 18 (cf. Fig. 13). The TKE is now more uniformly distributed and the individual velocity variances much closer to those of the LES, compared to those of S-2D-U.

The PBL still grows too fast (thin solid line in Fig. 12a), the streamwise velocity variance still produces too large of a local maxima near the surface and the PBL top, the spanwise velocity variance is underestimated, and the *w* variance peaks right at the mid-PBL; these are all persistent signatures of the 2D modeling.

Thus, for this shear convection case, to get the momentum transport correct, it is necessary to orient the 2D model domain perpendicular to the major shear direction. However, the model then cannot resolve the horizontal advection or the movement of the convective system, which may be important for deep convective systems with strong gravity wave effects. The quasi-3D idea proposed by Randall et al. (2003b), where two CRMs perpendicular to each other are used simultaneously, may help alleviate this problem.

5. Summary and conclusions

With the increasing use of the 2D modeling approach to represent atmospheric 3D convection, it is important to understand what the model really consists of, the physical aspects of its resolved 2D motion, and the reasons for its behavior. In this study we use a simple convective system—the dry convective PBL—to demonstrate how some statistical properties of 3D convection may be reasonably represented by a 2D turbulence model. The 2D model we adopt is a 2D version of the NCAR LES code where all *y* derivatives are set to 0. We use the LES as a baseline calculation to judge the performance of the 2D turbulence model results.

We first examine various statistical properties generated from the 2D model for a free convective PBL; some compare well with the LES and others do not. We offer physical interpretations of the similarities and differences. For example, the vertical distribution of the heat flux in the normalized height coordinate z/z_i (and hence fluxes of other conserved scalars, like moisture) is not very sensitive to the model dimensionality; the profile approaches linearity in height under quasi-equilibrium states, and hence, for a given surface flux, it depends only on the entrainment heat flux, which is somewhat energetically constrained and is unlikely to deviate too much from the expected value of ~ -0.2 of its surface value. So the overall vertical distribution of the heat flux (or vertical fluxes of other conserved variables) is likely to be reasonable from the 2D model.

As for the TKE, we show that to reproduce this quantity the 2D model requires a proper tuning of its SGS eddy viscosity and diffusivity. A proper amount of SGS eddy viscosity is needed to accomplish a proper amount of dissipation that cannot otherwise occur within 2D nonlinear dynamics. This strong dependence of TKE on SGS eddy viscosity is a major difference from LES; in LES, the total TKE should be controlled mainly by the surface heat flux (i.e., the external forcing), rather than by the SGS model. Using the SGS model described in section 2, we can simply tune the SGS eddy viscosity

parameter c_K in our 2D model, which controls the SGS eddy viscosity K_M through Eq. (4). This empirical tuning yields a ''proper'' eddy viscosity for the 2D turbulence model to reproduce the LES TKE; this proper SGS K_M is found to be on the same order as that in the LES, and much smaller than the ensemble-mean value.

Once the TKE in the free convective PBL is properly tuned, other statistics that are strongly tied to TKE can also be reasonably produced; this includes countergradient heat transport, surface friction velocity, and less satisfactorily, the vertical velocity variance, and hence convective mass flux. Because of the existence of a strong capping inversion, the 2D model also produces a characteristic eddy size on the order of the depth of the capping inversion, as in LES.

When vertical wind shear exists in the convection, the model orientation becomes another problem for 2D models. We show that when the 2D model domain is parallel to the mean shear, it generates an undesired countergradient momentum transport due to shear tilting of updrafts. This leads to a poor streamwise momentum flux, and therefore poor representations of mean wind profiles and all other wind related statistics, such as TKE and velocity variances. For the 2D model to reproduce the LES streamwise momentum flux, its numerical domain needs to be perpendicular to the major shear direction.

Calibration studies of 2D models, like the present one, can and should be systematically extended to consider clouds and deep convection and even hybrid configurations like the quasi-3D CRM approach proposed by Randall et al. (2003b).

The free convective PBL case has no preferred line or band structure in any horizontal direction, and hence the 2D convective plumes generated from the 2D model cannot be realized in nature and can only be interpreted as hypothetical plumes. Through proper tuning of SGS eddy viscosity, these model-generated hypothetical 2D plumes can behave somewhat like their 3D counterparts: random in space and time, carrying proper amounts of TKE and vertical fluxes, and having a characteristic eddy size (in both horizontal and vertical directions) on the order of the PBL depth if capped by an inversion. These 2D convective plumes provide a spatial and time varying structure (albeit somewhat artificial) that may be used for physical processes to interact upon on the time and space scales of convection, which is important for moist convection (e.g., spatial variation of cloud amount for radiation). This structure information is perhaps one of the most important advantages of 2D modeling over 1D modeling in parameterizing 3D convection.

Acknowledgments. We would like to thank Drs. Akio Arakawa, Wojciech Grabowski, Steve Krueger, and Peggy LeMone for their helpful comments.

REFERENCES

Ball, F. K., 1960: Control of inversion height by surface heating. *Quart. J. Roy. Meteor. Soc.,* **86,** 483–494.

Businger, J. A., and S. P. Oncley, 1990: Flux measurement with conditional sampling. *J. Atmos. Oceanic Technol.,* **7,** 349–352.

Deardorff, J. W., 1980: Stratocumulus-capped mixed layers derived from a three-dimensional model. *Bound.-Layer Meteor.,* **18,** 495–527.

Grabowski, W. W., and T. L. Clark, 1991: Cloud-environment interface instability: Rising thermal calculations in two spatial dimensions. *J. Atmos. Sci.,* **48,** 527–546.

——, and P. K. Smolarkiewicz, 1999: CRCP: A cloud resolving convection parameterization for modeling the tropical convective atmosphere. *Physica D,* **133,** 171–178.

——, X. Wu, and M. W. Moncrieff, 1996: Cloud-resolving modeling of tropical cloud systems during phase III of GATE. Part I: Two-dimensional experiments. *J. Atmos. Sci.,* **53,** 3684–3709.

——, ——, ——, and W. D. Hall, 1998: Cloud-resolving modeling of cloud systems during phase III of GATE. Part II: Effects of resolution and the third spatial dimension. *J. Atmos. Sci.,* **55,** 3264–3282.

Khairoutdinov, M. F., and D. A. Randall, 2001: A cloud-resolving model as a cloud parameterization in the NCAR Community Climate System model: Preliminary results. *Geophys. Res. Lett.,* **28,** 3617–3620.

Kopp, F. J., and H. D. Orville, 1994: The use of a two-dimensional, time-dependent cloud model to predict convective and stratiform clouds and precipitation. *Wea. Forecasting,* **9,** 62–77.

Krueger, S. K., 1988: Numerical simulation of tropical cumulus clouds and their interaction with the subcloud layer. *J. Atmos. Sci.,* **45,** 2221–2250.

——, and A. Bergeron, 1994: Modeling the trade cumulus boundary layer. *Atmos. Res.,* **33,** 169–192.

——, G. T. McLean, and Q. Fu, 1995: Numerical simulation of the stratus-to-cumulus transition in the subtropical marine boundary layer. Part II: Boundary-layer circulation. *J. Atmos. Sci.,* **52,** 2851–2868.

Lenschow, D. H., J. C. Wyngaard, and W. T. Pennell, 1980: Mean-field and second-moment budgets in a baroclinic, convective boundary layer. *J. Atmos. Sci.,* **37,** 1313–1326.

Lilly, D. K., 1962: On the numerical simulation of buoyant convection. *Tellus,* **14,** 152–172.

——, 1967: The representation of small-scale turbulence in numerical simulation experiments. *Proc. IBM Scientific Computing Symp. on Environmental Science,* Yorktown Heights, NY, Thomas J. Watson Research Center, 195–210.

——, 1986: The structure, energetics and propagation of rotating convective storms. Part I: Energy exchange with the mean flow. *J. Atmos. Sci.,* **43,** 113–125.

Moeng, C.-H., and J. C. Wyngaard, 1989: Evaluation of turbulent transport and dissipation closures in second-order modeling. *J. Atmos. Sci.,* **46,** 2311–2330.

——, and P. P. Sullivan, 1994: A comparison of shear- and buoyancy-driven planetary boundary layer flows. *J. Atmos. Sci.,* **51,** 999–1022.

——, and P. P. Sullivan, 2002: Large eddy simulation. *Encyclopedia of Atmospheric Sciences,* J. Holton, J. Pyle, and J. Curry, Eds., Academic Press, 1140–1150.

——, and Coauthors, 1996: Simulation of a stratocumulus-topped planetary boundary layer: Intercomparison among different numerical codes. *Bull. Amer. Meteor. Soc.,* **77,** 261–278.

Nieuwstadt, F. T. M., P. J. Mason, C.-H. Moeng, and U. Schumann, 1993: Large-eddy simulation of the convective boundary layer: A comparison of four computer codes. *Turbulent Shear Flows 8,* F. Durst et al., Eds., Springer-Verlag, 343–367.

Ogura, Y., 1962: Convection of isolated masses of buoyant fluid: A numerical calculation. *J. Atmos. Sci.,* **19,** 492–502.

Randall, D. A., and Coauthors, 2003a: Confronting models with data:

The GEWEX cloud systems study. *Bull. Amer. Meteor. Soc.*, **84,** 455–469.
——, M. Khairoutdinov, A. Arakawa, and W. W. Grabowski, 2003b: Breaking the cloud parameterization deadlock. *Bull. Amer. Meteor. Soc.*, **84,** 1547–1564.
Schmidt, H., and U. Schumann, 1989: Coherent structure of the convective boundary layer derived from large-eddy simulation. *J. Fluid Mech.*, **200,** 511–562.
Stevens, B., W. R. Cotton, and G. Feingold, 1998: A critique of one- and two-dimensional models of boundary layer clouds with a binned representation of drop microphysics. *Atmos. Res.*, **47–48,** 529–553.
Tao, W.-K., J. Simpson, and S.-T. Soong, 1987: Statistical properties of a cloud ensemble: A numerical study. *J. Atmos. Sci.*, **44,** 3175–3187.
Tennekes, H., 1973: A model for the dynamics of the inversion above a convective boundary layer. *J. Atmos. Sci.*, **30,** 558–567.
Tompkins, A. M., 2000: The impact of dimensionality on long-term cloud-resolving model simulations. *Mon. Wea. Rev.*, **128,** 1521–1535.
Willis, G. E., and J. W. Deardorff, 1974: A laboratory model of the unstable planetary boundary layer. *J. Atmos. Sci.*, **31,** 1297–1307.
——, and ——, 1979: Laboratory observations of turbulent penetrative-convection planforms. *J. Geophys. Res.*, **84,** 295–302.
Wyant, M. C., C. S. Bretherton, H. A. Rand, and D. E. Stevens, 1997: Numerical simulations and a conceptual model of the subtropical marine stratocumulus to trade cumulus transition. *J. Atmos. Sci.*, **54,** 168–192.
Wyngaard, J. C., 1992: Atmospheric turbulence. *Annu. Rev. Fluid Mech.*, **24,** 205–233.
——, and C.-H. Moeng, 1992: Parameterizing turbulent diffusion through the joint probability density. *Bound.-Layer Meteor.*, **60,** 1–13.
Xu, K.-M., and D. A. Randall, 1996: Explicit simulation of cumulus ensembles with the GATE phase III data: Comparison with observations. *J. Atmos. Sci.*, **53,** 3710–3736.
——, A. Arakawa, and S. K. Krueger, 1992: The macroscopic behavior of cumulus ensembles simulated by a cumulus ensemble model. *J. Atmos. Sci.*, **49,** 2402–2420.